Pyridoxal-5′-phosphate–dependent bifunctional enzyme catalyzed biosynthesis of indolizidine alkaloids in fungi

Guang Zhi Dai[a,1], Wen Bo Han[a,1], Ya Ning Mei[b], Kuang Xu[a], Rui Hua Jiao[a], Hui Ming Ge[a], and Ren Xiang Tan[a,c,2]

[a]State Key Laboratory of Pharmaceutical Biotechnology, Institute of Functional Biomolecules, School of Life Sciences, Nanjing University, 210023 Nanjing, China; [b]Department of Clinical Laboratory, The First Affiliated Hospital of Nanjing Medical University, 210029 Nanjing, China; and [c]State Key Laboratory Cultivation Base for Traditional Chinese Medicine Quality and Efficacy, Nanjing University of Chinese Medicine, 210023 Nanjing, China

Edited by Sang Yup Lee, Korea Advanced Institute of Science and Technology, Daejeon, Korea (South), and approved December 2, 2019 (received for review August 25, 2019)

Indolizidine alkaloids such as anticancer drugs vinblastine and vincristine are exceptionally attractive due to their widespread occurrence, prominent bioactivity, complex structure, and sophisticated involvement in the chemical defense for the producing organisms. However, the versatility of the indolizidine alkaloid biosynthesis remains incompletely addressed since the knowledge about such biosynthetic machineries is only limited to several representatives. Herein, we describe the biosynthetic gene cluster (BGC) for the biosynthesis of curvulamine, a skeletally unprecedented antibacterial indolizidine alkaloid from *Curvularia* sp. IFB-Z10. The molecular architecture of curvulamine results from the functional collaboration of a highly reducing polyketide synthase (CuaA), a pyridoxal-5′-phosphate (PLP)-dependent aminotransferase (CuaB), an NADPH-dependent dehydrogenase (CuaC), and a FAD-dependent monooxygenase (CuaD), with its transportation and abundance regulated by a major facilitator superfamily permease (CuaE) and a Zn(II)Cys_6 transcription factor (CuaF), respectively. In contrast to expectations, CuaB is bifunctional and capable of catalyzing the Claisen condensation to form a new C–C bond and the α-hydroxylation of the alanine moiety in exposure to dioxygen. Inspired and guided by the distinct function of CuaB, our genome mining effort discovers bipolamines A–I (bipolamine G is more antibacterial than curvulamine), which represent a collection of previously undescribed polyketide alkaloids from a silent BGC in *Bipolaris maydis* ATCC48331. The work provides insight into nature's arsenal for the indolizidine-coined skeletal formation and adds evidence in support of the functional versatility of PLP-dependent enzymes in fungi.

indolizidine alkaloid | biosynthesis | O_2 and PLP-dependent enzyme | genome mining | antibacterial activity

Structurally unique and biologically potent natural products biosynthesized in microorganisms and others are a promising source for lead compounds that may energize the discovery of new drugs and agrochemicals (1, 2). Among them, the indolizidine alkaloids with the fused 5- and 6-membered cycles sharing a nitrogen atom seem to be highly attractive due to their intriguing structure and promising bioactivity (e.g., antibacterial, antiinflammatory, and antitumor) (Fig. 1) (3–5) as well as their elusive involvement in the producers' chemical defense (6, 7). In particular, the medicinal value of some indolizidine alkaloids was showcased by the marketed anticancer drugs vinblastine and vincristine (Fig. 1*A*). Motivated by the observation, many groups have developed approaches to expand the chemical space of this family of alkaloids with an intention of hitting more prominent molecules (5, 8–10). Meanwhile, the diversity landscape of natural polyketide alkaloids suggests the biosynthetic versatility by the species belonging to different kingdoms (3, 4, 11).

In plants, the formation of indolizidine frameworks is proposed to result from the L-lysine metabolism (*SI Appendix*, Fig. S1) (12). In actinomycetes and fungi, the construction of indolizidine moieties involves the reductive release of the polyketide chain as an aldehyde followed by a reductive amination step (13–16), as exemplified by the biosynthesis of cyclizidine and swainsonine in *Streptomyces* NCIB 11646 and *Metarhizium robertsii* ARSEF23 (*SI Appendix*, Fig. S1) (13–16), respectively. However, the biosynthetic mechanism of indolizidine motif construction in nature remains incompletely addressed. In particular, the described skeletal construction patterns seem to be insufficient to rationalize the biosynthesis of curvulamine (antibacterial) and curindolizine (antiinflammatory) (numbered **1** and **2** in Fig. 1*C*, respectively) 2 highly diversified bioactive indolizidine alkaloids isolated from the culture of *Curvularia* sp. IFB-Z10 associated with the white croaker (*Argyrosomus argentatus*) (17, 18). Furthermore, the bioactivity of **1** and **2** is, at least partly, associated with the indolizidine moiety. The observation intensified our curiosity about the curvulamine (**1**) biosynthesis in the fungus, which might showcase another mechanism for constructing polyketide alkaloids in nature.

Significance

Indolizidine alkaloids are widespread in nature, diverse in structure, prominent in bioactivity, and elusive in ecology, but only a few have been biosynthetically clarified. Here, we describe the biosynthesis of curvulamine, a unique antibacterial indolizidine alkaloid from *Curvularia* sp. IFB-Z10. Unexpectedly, curvulamine results from a consortium of 6 enzymes including a pyridoxal-5′-phosphate (PLP)-dependent bifunctional aminotransferase (CuaB) catalyzing the formation of C–C (via Claisen condensation) and C–O bonds (using dioxygen). Guided by the CuaB function, our genome mining effort revealed, from a single silent gene cluster, a collection of previously undescribed polyketide alkaloids with 1 more antibacterial than curvulamine. Collectively, the work describes an unprecedented construction of indolizidine-coined skeletons and provides another layer of the functional versatility to the PLP-dependent enzymes.

Author contributions: G.Z.D., W.B.H., and R.X.T. designed research; G.Z.D., W.B.H., Y.N.M., K.X., and R.H.J. performed research; G.Z.D., W.B.H., H.M.G., and R.X.T. analyzed data; and G.Z.D., W.B.H., and R.X.T. wrote the paper.

The authors declare no competing interest.

This article is a PNAS Direct Submission.

Data deposition: The crystallography data reported in this paper have been deposited in the Cambridge Crystallographic Data Centre, https://ccdc.cam.ac.uk (accession nos. CCDC-1565933, CCDC-994365, CCDC-954855, CCDC-995222, CCDC-954856, CCDC-994366, and CCDC-994364). Sequence data have been deposited in GenBank, https://www.ncbi.nlm.nih.gov/genbank (accession nos. MN379757–MN379762).

[1]G.Z.D. and W.B.H. contributed equally to this work.

[2]To whom correspondence may be addressed. Email: rxtan@nju.edu.cn.

This article contains supporting information online at https://www.pnas.org/lookup/suppl/doi:10.1073/pnas.1914777117/-/DCSupplemental.

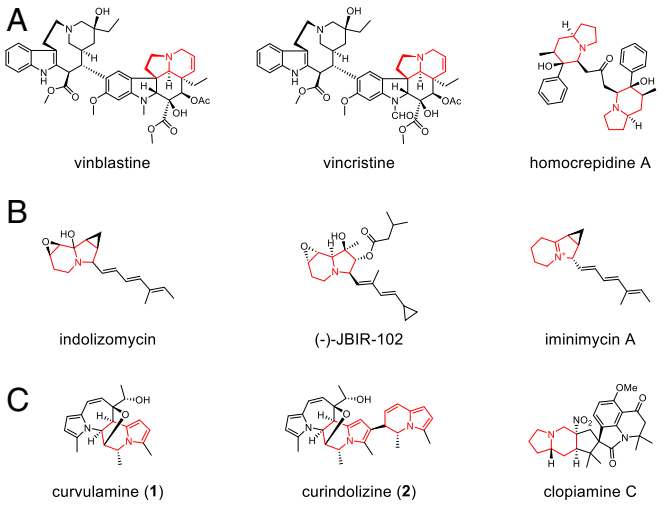

Fig. 1. Representative indolizidine alkaloids from: (*A*) plants (vinblastine, vincristine, and homocrepidine A); (*B*) actinomycetes (indolizomycin, (-)-JBIR-102, and iminimycin A); and (*C*) fungi [curvulamine (**1**), curindolizine (**2**), and clopiamine C].

Our isotope-labeled precursor feeding experiments and the enzyme inhibition test indicated that the fungal production of **1** requires the coinvolvement of polyketide synthase (PKS) and pyridoxal-5′-phosphate (PLP)-dependent 8-amino-7-oxononanoate synthase (AONS) (17). Starting from the findings, the present work deciphers the biosynthetic gene cluster of **1** via a combination of genome sequencing, gene mutation, heterologous expression, and enzymatic characterization. To our anticipation, the biosynthesis of **1** symbolizes an undescribed type of generating indolizidine moiety with the fungal PLP-dependent enzyme (designated herein as CuaB) playing bifunctional roles in catalyzing both the C–C bond formation and the α-hydroxylation of the alanine residue.

Results and Discussion

Identification of the Curvulamine Biosynthetic Gene Cluster and Its On-Pathway Intermediates. In an attempt to get an insight into the curvulamine (**1**) biosynthesis, we performed the whole genome sequencing of *Curvularia* sp. IFB-Z10, which produces **1** as a major polyketide alkaloid. We analyzed the sequenced genome by the antibiotics and secondary metabolite analysis shell (antiSMASH) (fungal version) to reveal that this strain contains at least 27 biosynthetic gene clusters (BGCs) (*SI Appendix*, Fig. S2) (19). In reminiscence of the fact that PKSs are essential for the skeletal construction of polyketide alkaloids (13–16), our attention was first focused on the 10 *pks*-containing BGCs (designated as *pks1-10*) (*SI Appendix*, Fig. S2). Thus, the RT-qPCR experimentation was conducted to analyze the mRNA expression levels of the *pks* genes in the Czapek-Dox liquid medium that allows the wild-type (WT) strain of *Curvularia* sp. IFB-Z10 to produce **1** as an abundant secondary metabolite (*SI Appendix*, Fig. S3*A*). As a result, the mRNA expression levels of *pks4*, *pks5*, and *pks10* (designated as *cuaA*) were obviously higher than those of others (*SI Appendix*, Fig. S3*B*). Adjacent to *cuaA* is a gene (designated as *cuaB*) that encodes a PLP-dependent aminotransferase (Fig. 2*A* and *SI Appendix*, Table S1). Deletion of *cuaA* and *cuaB* completely abolished the production of **1** (*SI Appendix*, Fig. S3*C*). But the *Δpks4* and *Δpks5* mutants formed **1** as did the WT strain (*SI Appendix*, Fig. S3*C*). Thus, the biosynthesis of **1** requires the *cuaA* and *cuaB* genes, but not *pks4* or *pks5* genes.

In view of the disappearance of **1** in *ΔcuaA* and *ΔcuaB* mutants, our attention was drawn to the *cuaA*- and *cuaB*-containing BGC (hereafter referred to as the *cua* gene cluster) which was found in scaffold 8. The *cua* gene cluster includes 4 additional genes that encode respectively a short-chain alcohol dehydrogenase (CuaC), a FAD-dependent monooxygenase (CuaD), a major facilitator superfamily permease (CuaE), and a Zn(II)Cys_6 transcription factor (CuaF) (Fig. 2*A* and *SI Appendix*, Table S1). To ascertain gene cluster boundary, we constructed *ΔORF1-3*, *ΔcuaC-F*, and *ΔORF10-12* mutants (*SI Appendix*, Fig. S4*A*). The high-performance liquid chromatography (HPLC) analysis of the mutant cultures showed that the *ΔORF1-3* and *ΔORF10-12* strains produced **1** as did the WT strain (*SI Appendix*, Fig. S4*B*), underscoring that *ORF1* and *ORF12* were the left and right boundaries of the *cua* gene cluster, respectively. Moreover, **1** failed to be detected in the *ΔcuaE* and *ΔcuaF* mutant cultures (Fig. 2*B*, traces *iv* and *v*), reinforcing their functional roles in the efficient transportation and up-regulated expression of **1** as annotated by the bioinformatics analysis.

With the gene function ascertained, we were curious to identify the intermediates that may be suggestive of biosynthetic steps toward **1**. Our attention was first directed to the products of the *ΔcuaC* and *ΔcuaD* mutants. The *ΔcuaC* mutant was unable to produce **1** but capable of forming **3** and **4** (Fig. 2*B*, trace *vii*). Due to its instability, **3** could only be isolated under the protection of dry ice and without any light exposure. Compound **3** was evidenced to have a molecular formula of $C_{10}H_{13}NO_2$ from its Na^+-liganded molecular ion at *m/z* 202.0843 ($C_{10}H_{13}NO_2Na$ requires 202.0839) in its high-resolution electrospray ionization mass spectrometry (HR-ESI-MS) spectrum. Subsequent interpretation of its 1D (^1H and ^{13}C) and 2-dimensional (2D) NMR spectra (^1H-^1H chemical shift correlation spectroscopy [COSY], heteronuclear singular quantum correlation [HSQC], and heteronuclear multiple-bond coherence [HMBC]) indicated that **3** was 2-hydroxy-2-methyl-5-((1*E*,3*E*)-penta-1,3-dien-1-yl)-1,2-dihydro-3*H*-pyrrol-3-one (Fig. 3 and *SI Appendix*, Table S5 and Figs. S16–S20). Compound **4** was found to have a molecular formula of $C_{10}H_{13}NO_3$ according to its Na^+-liganded molecular ion at *m/z* 218.0784 ($C_{10}H_{13}NO_3Na$ requires 218.0788) in its HR-ESI-MS spectrum, underscoring that **4** was a monooxygenated derivative of **3**. The same set of 1-dimensional (1D) and 2D NMR spectra

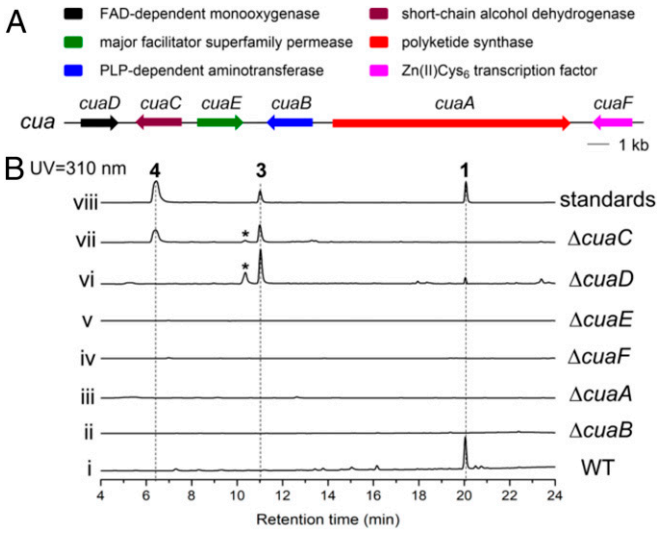

Fig. 2. Identification of the curvulamine (**1**) biosynthetic gene cluster. (*A*) The putative *cua* biosynthetic gene cluster in *Curvularia* sp. IFB-Z10. CuaA: polyketide synthase; CuaB: PLP-dependent bifunctional aminotransferase; CuaC: short-chain alcohol dehydrogenase; CuaD: FAD-dependent monooxygenase; CuaE: major facilitator superfamily permease; CuaF: Zn(II)Cys_6 transcription factor. (*B*) HPLC profiling for alkaloids produced by the 6 mutants (*ΔcuaA–ΔcuaF*) and the WT strain. *, unidentified minor metabolites.

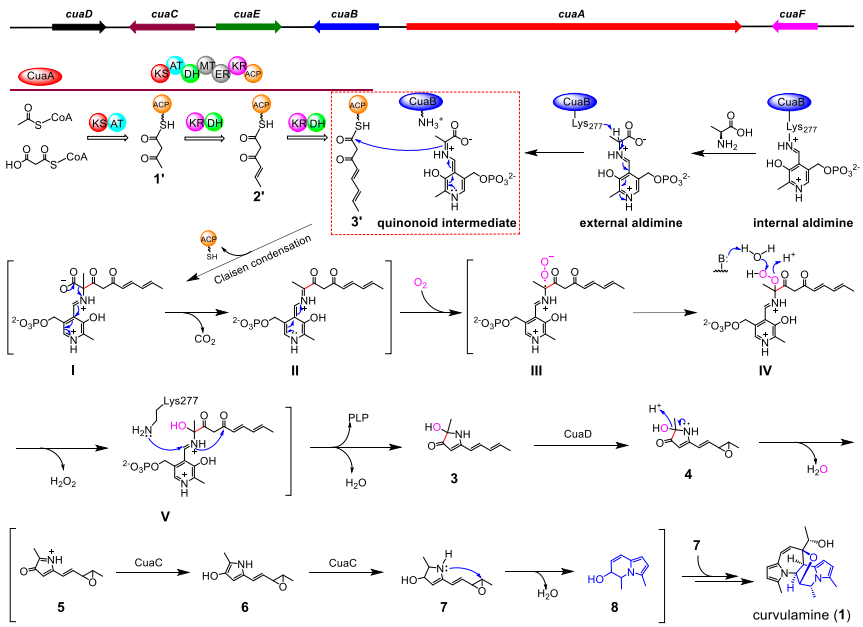

Fig. 3. Proposed curvulamine (**1**) biosynthetic pathway based on gene mutation, heterologous expression, and enzymatic assay. CuaB, a bifunctional aminotransferase, catalyzes the formation of both C–C (via Claisen condensation) and C–O bonds in the presence of O_2.

of **4** confirmed that it was 2,3-epoxide of **3** (Fig. 3 and *SI Appendix*, Table S6 and Figs. S21–S25). Complementation of **3** and **4** to Δ*cuaA* and Δ*cuaB* mutants restored the production of **1**, indicating that both are the on-pathway intermediates (*SI Appendix*, Fig. S5). The Δ*cuaD* mutant generated **3** as well, but along with a reduced abundance of **1** (Fig. 2*B*, trace *vi*). The residual amount of **1** produced by the Δ*cuaD* strain (Fig. 2*B*, trace *vi*) highlighted the presence of presumable CuaD homolog(s) outside the *cua* gene cluster as encountered in the L-*allo*-isoleucine biosynthesis (20).

Heterologous Expression of CuaA, CuaB, and CuaD in *Aspergillus oryzae* and *Saccharomyces cerevisiae*. The production of **3** and **4** by the Δ*cuaC* mutant prompted us to hypothesize that CuaA and CuaB might be involved in the nascent stage of the **1** biosynthesis. To confirm the assumption, we conducted the heterologous coexpression of *cuaA* and *cuaB* in *Aspergillus oryzae* NSAR1 and *Saccharomyces cerevisiae* BJ5454-NpgA (*cuaA* and *cuaB* without introns) (21–23). As expected, **3** formed in the 2 hosts after a 3-d fermentation (Fig. 4*A*, traces *ii* and *iv*). The structural feature of **3** agrees with the bioinformatic analysis suggesting that methyltransferase and enoyl reductase domains of CuaA are inactive (*SI Appendix*, Fig. S6) (24). These results confirmed that the *cuaA* and *cuaB* genes are responsible for the early-stage biosynthesis of **1** with the on-pathway intermediate **3** produced via a consortium of CuaA and CuaB (Fig. 3). This is another example of PLP-dependent polyketide chain release involved in the natural product biosynthesis (25).

With the finding, we speculated the FAD-dependent monooxygenase CuaD might be responsible for the conversion of **3** into **4**. The recombinant CuaD protein was overexpressed in *Escherichia coli trans*etta (DE3) and purified as a yellow protein with FAD as the cofactor (*SI Appendix*, Fig. S7). Exposure of CuaD to **3**, FAD, and NADH led to the complete transformation of **3** into **4** over a prolonged reaction time (Fig. 4*B*, traces *i–iii*). We also coexpressed *cuaA*, *cuaB*, and *cuaD* in *A. oryzae* NSAR1 to reinforce the in vivo production of **4** (Fig. 4*A*, trace *v*). The above experiments established CuaD as a monooxygenase that catalyzes the 2,3-epoxidation of **3** to form **4** (Fig. 3). Next, we tried to characterize the function of CuaC, annotated as short-chain alcohol dehydrogenase. Unfortunately, the CuaC protein could not be obtained in a soluble form after many attempts. However, the accumulation of **4** by the Δ*cuaC* mutant (Fig. 2*B*, trace *vii*) could be rationalized only by assuming that CuaC is likely involved in the further modification of **4** (Fig. 3). Presumably, a proton-promoted dehydration of **4** gives **5**, which is transformable into **6** after ketoreduction (26). The keto–enol tautomerization of **6** allows a second-round ketoreduction to form **7**, whose nitrogen atom attacks the epoxide carbon to yield **8** after dehydration. Further tailoring of **8** affords **1** (Fig. 3). The proposed function of CuaC gained a reinforcement from its

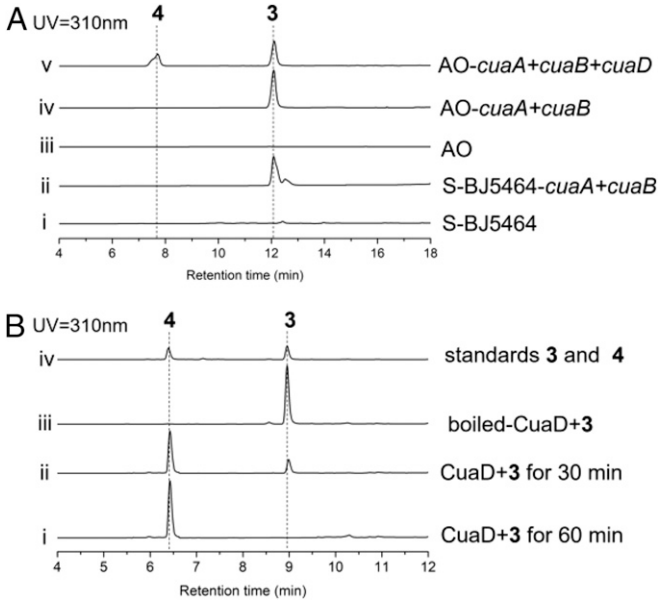

Fig. 4. Heterologous expression of *cuaA*, *cuaB*, and *cuaD*. (*A*) HPLC profilings (recorded at 310 nm) for **3** and **4** produced in *A. oryzae* (AO) and *S. cerevisiae* (S-BJ5464). (*B*) CuaD (100 μM) catalyzes the conversion of **3** into **4** in the 50-mM PBS buffer (pH 7.2).

homolog RhlG (31% identity to CuaC), a NADPH-dependent β-ketoacyl reductase of short-chain alcohol dehydrogenase/reductase (SDR) superfamily catalyzing the ketoreduction steps in the biosynthesis of rhamnolipid (27).

Biochemical Characterization of CuaB. As confirmed by the heterologous expression in *A. oryzae* and *S. cerevisiae* BJ5454-NpgA, the coinvolvement of CuaA and CuaB in the production of **3** motivated us to understand the biochemical feature of CuaB. Therefore, we expressed CuaA (276 kDa) in *S. cerevisiae* BJ5454-NpgA and the recombinant CuaB in *E. coli trans*etta (DE3) (*SI Appendix*, Fig. S8*A*). The purified CuaB is a yellow holoenzyme with a characteristic absorbance maximum at 425 nm, indicating the formation of internal aldimine by combining with the PLP cofactor (*SI Appendix*, Fig. S8*B*) (28). Then equimolar amounts (100 μM) of CuaA and CuaB were incubated at 30 °C for 10 h with the substrates (L-alanine [1 mM], acetyl-CoA [2 mM], and malonyl-CoA [2 mM]) in the presence of NADPH (4 mM) and PLP (1 mM). After being quenched by adding acetonitrile, the liquid chromatography–mass spectrometry (LC-MS) analysis of the reaction mixture indicated the production of **3** (Fig. 5*A*, trace *vi*). At this stage, our attention was drawn to the unusual hydroxylation of C9 in **3** (Fig. 3). The reported PLP-dependent Claisen condensation between polyketide chain or acyl-CoA and amino acids results in the formation of a new C–C bond as discerned in the biosynthesis of undecylprodigiosin, fumonisin B1, and saxitoxin (29–31). Nevertheless, the α-hydroxylation of amino acid residue was not observed. The α-hydroxylation of the on-pathway intermediate **3** suggests an unusual catalytic mechanism of CuaB, which might be fundamental to the construction pattern for the indolizidine skeleton. In order to verify whether CuaB is responsible for the α-hydroxylation of alanine residue of **3**, we synthesized the substrates, (4*E*,6*E*)-3-oxoocta-4,6-dienoyl-*N*-acetylcysteamine (numbered **S5**) (*SI Appendix*, Figs. S26–S28) and (4*E*,6*E*)-3-oxoocta-4,6-dienoyl-SCoA (numbered **S13**) (*SI Appendix*, Figs. S29–S33), to mimic the acyl carrier protein (ACP)-bound tetraketide (**3′**, Fig. 3). The reaction of **S5** and L-alanine was performed with exposure to CuaB and PLP, but no production of **3** was revealed by the LC-MS analysis (Fig. 5*A*, trace *i*), suggesting that **S5** could not efficiently mimic the biosynthetic step. Therefore, we expressed the ACP domain of CuaA and phosphopantetheinyl transferase (PPTase) NpgA in *E. coli trans*etta (DE3) (*SI Appendix*, Fig. S9*A*). A 340-Da shift was observed by the matrix-assisted laser desorption/ionization time-of-flight mass spectrometer (MALDI-TOF-MS) analysis after the incubation of the *apo* CuaA-ACP and CoA using NpgA, indicating that *apo* CuaA-ACP was converted into its *holo* form (*SI Appendix*, Fig. S9*B*). In addition, **S13** was also confirmed to be accommodated by *holo* CuaA-ACP by the observed 136-Da increment in the molecular weight (*SI Appendix*, Fig. S9*B*). The substrate **S13** and L-alanine were incubated with CuaB in the presence of *apo* CuaA-ACP, NpgA, and PLP. Satisfactorily, **3** was produced as detected by the LC-MS analysis (Fig. 5*A*, trace *iv*). These results indicated that the coparticipation of CuaA and CuaB was important for the recognition of substrate and subsequent catalysis.

Next, we were curious about the origination of the hydroxyl group in **3**. Thus, **S13** was subjected to an anaerobic conversion test, but it failed to form **3** (Fig. 5*A*, trace *ii*). This suggests that dioxygen was likely indispensable for the catalytic ability of CuaB. To reinforce the assumption, we conducted separately the isotope-labeling experiments using $^{18}O_2$ and $H_2{}^{18}O$. As indicated by the LC-MS analysis, ^{18}O-**3*** (**3** labeled with an ^{18}O atom) generated in the presence of $^{18}O_2$ and displayed its $[M+Na]^+$ ion at *m/z* 204, which has a 2-Da increment from that of **3** formed in exposure to $^{16}O_2$ (Fig. 5 *B*, *i* and *iii*). Therefore, the hydroxyl oxygen of **3** is derived from dioxygen, not from water. PLP is a versatile cofactor which is involved in a wide range of reactions as reviewed recently (32). To our knowledge, a total of 4 PLP-dependent enzymes are noticed to activate O_2 to complete challenging reactions including the oxidation of inert C–C bonds (*SI Appendix*, Fig. S10) (33–36). To validate the possible catalytic residues of CuaB, the site-directed mutagenesis experiments were conducted. For the PLP-dependent AONSs, the active site residues including His, Ser, Aps, Thr, and Lys are important for the AONSs to catalyze the C–C bond formation through the decarboxylative condensation between an amino acid and an acyl-CoA (28, 37). Similarly, the multiple sequence alignment indicated H158, S214, D243, H246, T274, and K277 in CuaB are also conserved (*SI Appendix*, Fig. S11). The purified CuaB-K277A mutant is colorless and inactive (Fig. 5*A*, trace *iii* and *SI Appendix*, Fig. S8*B*), indicating K277 covalently binds the PLP cofactor to generate internal aldimine (Fig. 3). The H158A, S214A, and T274A mutations extremely decreased the activity of CuaB (*SI Appendix*, Fig. S13). However, H246 seems inessential for the enzymatic function since the CuaB-H246A mutant was shown to be as active as CuaB (*SI Appendix*, Fig. S13). Interestingly, a total of 12 polar amino acids (K199, K202, R203, D266, H337, H367, E368, D369, H373, E374, T378, and H379) were distinctly conserved in CuaB and its homologous proteins, but not in PLP-dependent AONSs (*SI Appendix*, Fig. S11). Furthermore, E368 and H373 are particularly essential for the discerned CuaB function because CuaB-E368A and CuaB-H373A

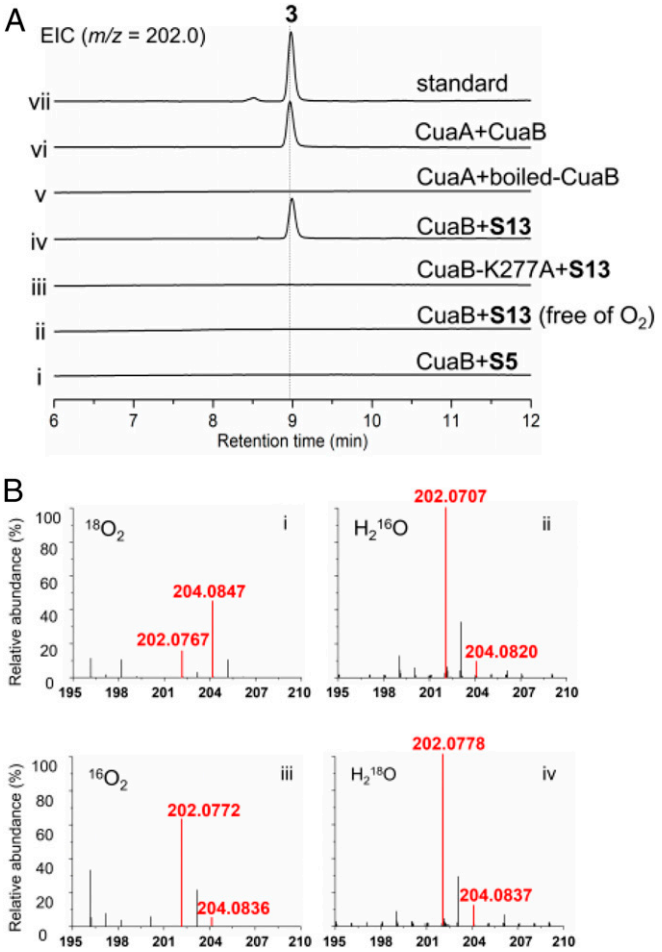

Fig. 5. Biochemical characterization of CuaB with PLP as a cofactor. (*A*) LC-MS profilings for the CuaB catalyzed transformation of **S13** or **S5**. (*B*) LC-MS analysis of the CuaB-transformed products (**3** with and without ^{18}O atom) in exposure to $^{18}O_2$ (*i*) and $H_2{}^{16}O$ (*ii*), and to $^{16}O_2$ (*iii*) and $H_2{}^{18}O$ (*iv*).

mutants were demonstrated to have sharply reduced catalytic activity (*SI Appendix*, Fig. S13). Collectively, the amino acid residues H158, S214, T274, K277, E368, and H373 are important for the CuaB function. In addition, our phylogenic analysis indicated that CuaB and its homologs are located in the same clade (Fig. 6) but separated from AONSs and other PLP-dependent oxidases (33–36, 38, 39). Accordingly, CuaB showcases an undescribed family of PLP-dependent bifunctional enzymes that catalyzes both the C–C bond formation and activates O_2 via a hydroperoxide-PLP adduct to complete the α-hydroxylation of amino acid residue. With the finding, we were curious about whether other enzymes in this clade can perform the same/similar catalytic function as does CuaB. Therefore, we overexpressed and purified the XP_007700279.1 protein from *Bipolaris sorokiniana* ND90Pr (designated as CuaB-H1 with 90% similarity and 83% identity to CuaB) and the XP_007711337.1 protein from *Bipolaris zeicola* 26-R-13 (designated as CuaB-H2 with 90% similarity and 84% identity to CuaB). As expected, the 2 enzymes did catalyze the conversion of **S13** into **3** as indicated by LC-MS analysis (*SI Appendix*, Fig. S8*C*).

In view of biotin biosynthesis (28), the K277 residue in CuaB could be proposed to bind to the PLP cofactor to form the internal aldimine (Fig. 3), which is subsequently exchanged with L-alanine to generate external aldimine. Specifically, K277 despoils the C_α-proton of the external aldimine to yield the quinonoid intermediate, which primes the tetraketide chain-tethering ACP to form intermediate I via Claisen condensation (Fig. 3). Decarboxylation of I gave the quinonoid carbanion complex II. An electron derived from II is transferred to O_2 to produce radical aldimine and superoxide anion complex III, which tends to form a hydroperoxide-PLP adduct IV. These processes were adopted for reasoning the biosynthetic pathways of celesticetin and capuramycin (33, 34). Most likely, the water attacks the peroxy bond of IV to complete the hydroxylation of V with the elimination of H_2O_2 in analogy with the proposals for the PLP- and O_2-codependent oxidations (32). The amino nitrogen atom in V was apt to nucleophilically attack the conjugated carbonyl group to give **3** after the release of PLP and water (Fig. 3). This rationalization was reinforced by the reaction assay based on the principle of the H_2O_2 oxidation-triggered fluorescent liberation within a few seconds and the production of H_2O_2 in stoichiometric amounts (*SI Appendix*, Fig. S12) (40).

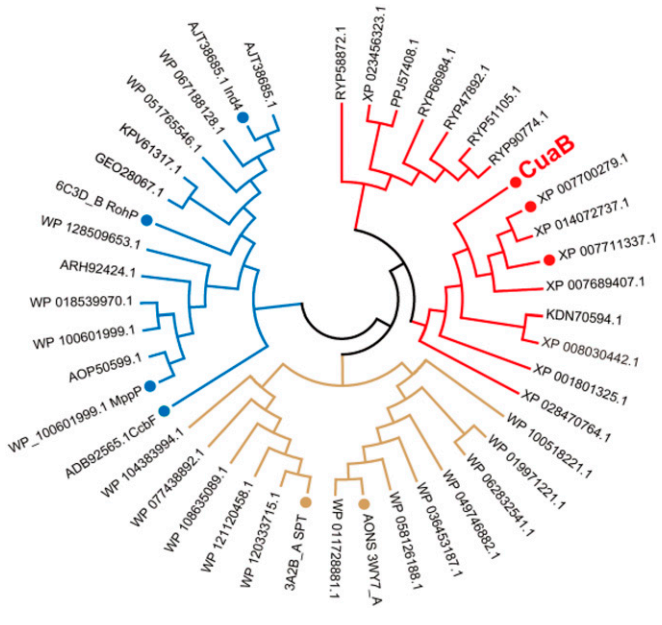

Fig. 6. The phylogenetic tree of CuaB and its homologs. CuaB, XP_007711337.1, and XP_007700279.1 (solid circle in red) located in a distinct clade can catalyze both the C–C bond formation (via Claisen condensation) and α-hydroxylation of alanine residue employing O_2. This is functionally different from other PLP-dependent enzymes such as PLP-dependent oxidases CcbF, MppP, RohP, and Ind4 (solid circle in blue) that catalyze oxidation (33–36), and L-serine palmitoyltransferase (SPT) and AONS (solid circle in yellow) catalyze the C–C bond formation via the Claisen condensation of acyl-CoA with α-amino acids (38, 39). The sequence alignment was analyzed by Clustalw and the phylogenetic tree was constructed by the neighbor-joining method using MEGA 7.0 software.

Genome Mining for New Antibacterial Indolizidine Alkaloids. Many new bioactive polyketide alkaloids are thought to exist in nature as "hidden" natural products, since their gene clusters keep silent in laboratory conditions (41). Inspired and guided by the distinctness of CuaB involved in the biosynthesis of curvulamine (**1**), an antibacterial polyketide alkaloid (17) (Fig. 6), a genome mining effort was performed to search for the homologous BGCs in fungal genomes available in the National Center for Biotechnology Information (NCBI) and Joint Genome Institute (JGI) databases. After AntiSMASH analysis, 5 BGCs were shown to be similar to the *cua* gene cluster that encodes the typical enzymes (*SI Appendix*, Fig. S14*A*) required for the biosynthesis of curvulamine-like indolizidine alkaloids. Furthermore, such genome mining allowed us to recognize 5 more distinct BGCs that encode, in addition to the CuaB-like enzyme, a set of different tailoring enzymes including cytochrome P450 monooxygenase, cofactor F_{420}-dependent oxidoreductase, and α-ketoglutarate–dependent oxygenase (*SI Appendix*, Fig. S14*B*). These BGCs were therefore anticipated to synthesize novel polyketide alkaloids. Among them, the homologous *bip* gene cluster in *Bipolaris maydis* ATCC48331 (Fig. 7*A* and *SI Appendix*, Table S2) was expected to be prominent in constructing polyketide alkaloids. In contrast to our expectation, no polyketide alkaloid was detectable in the *B. maydis* culture in different media (Fig. 7*B*, traces *i*–*viii* and *SI Appendix*, Table S16), suggesting the assumed *bip* gene cluster was likely silent in the laboratory condition (Fig. 7*B*, traces *i*–*viii*). After scrutinizing the *cua* and *bip* gene clusters (*SI Appendix*, Table S2), we noticed and overexpressed the putative transcription factor *bipF* (52% identity to *cuaF*) using a strong α-amylase (*amyB*) promoter to activate the *bip* gene cluster (Fig. 7*B*, trace *ix*). The cultivation of the *B. maydis* (OE::*bipF*) strain was scaled up, and the ethyl acetate extract was fractionated to afford 9 new polyketide alkaloids we have named bipolamines A–I (**14**–**22**) (Fig. 7*B*). The structure and absolute stereochemistry of **14** to **22** were unequivocally assigned by a combination of their 1D (^{1}H and ^{13}C) and 2D NMR spectra (^{1}H-^{1}H COSY, HSQC, HMBC, and NOESY) and single crystal X-ray diffraction (*SI Appendix*, Tables S7–S15 and Figs. S35–S92). In agreement with the gene organization, **14** to **22** are all polyketide alkaloids (Fig. 7*B*).

Inspired by the bacterial growth inhibition of curvulamine (**1**) (17), **14** and **17** to **22** were evaluated for the antibacterial action against pathogens *Veillonella parvula*, *Actinomyces israelii*, *Streptococcus* sp., *Peptostreptococcus* sp., and *Bacteroides vulgates*. Gratifyingly, bipolamine G (**20**) was shown to be more potent than **1** (*SI Appendix*, Table S17). Due to the instability, **15** and **16** decomposed prior to the antibacterial assay. This result is supportive of the conserved mechanism for the polyketide alkaloid construction in fungi and demonstrates that the genome mining strategy is effective for the discovery of new bioactive natural products biosynthesized by silent gene clusters.

Indolizidine alkaloids are widespread in nature since they can be biosynthesized by many plant species and microbial strains (3, 4). Some animal species such as toads also "produce" toxic indolizidine alkaloids by utilization of alkaloid-containing prey for the sake of maintaining the chemical defense (6). Thus, there might be an unforeseeable versatility of the indolizidine alkaloid

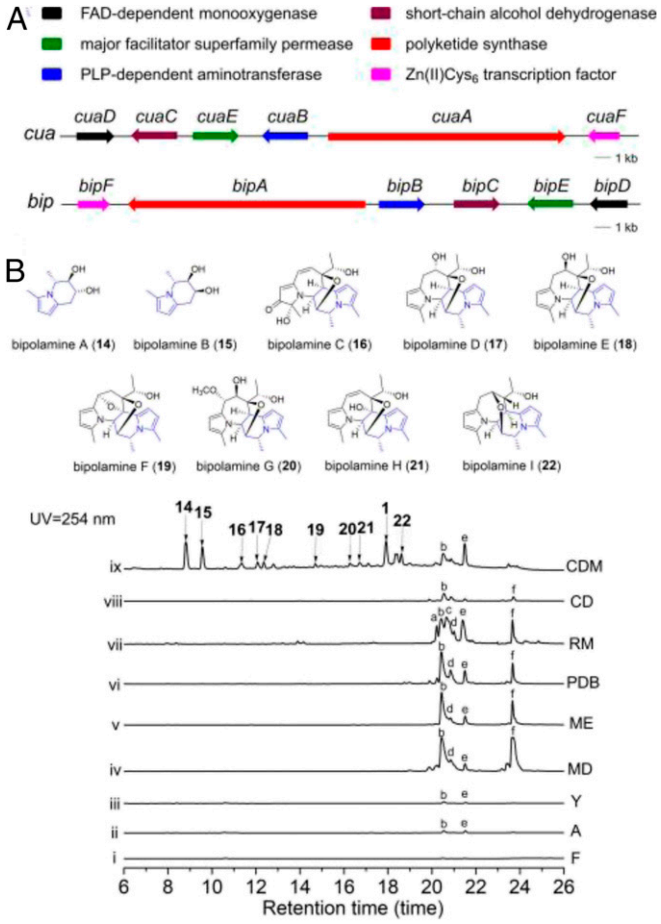

Fig. 7. Genome mining for new polyketide alkaloids from the silent *bip* cluster in *B. maydis* ATCC48331. (*A*) Comparison between the *cua* and *bip* clusters. (*B*) HPLC profilings of the EtOAc extracts derived from the *B. maydis* cultures in different media. The silent *bip* cluster was activated by overexpressing transcription factor BiF, leading to characterization of new alkaloid bipolamines A–I (**14**–**22**). *, Nonalkaloidal secondary metabolites (*a*–*f*) ascertained by the LC-HR-ESI-MS analysis (*SI Appendix*, Table S18).

biosynthesis in different organisms. This is substantiated by the present study that reveals an undescribed construction of the indolizidine nucleus of curvulamine (**1**) in *Curvularia* sp. IFB-Z10. Our attention to the biosynthetic gene cluster of **1** led to the identification of CuaB as a bifunctional PLP-dependent aminotransferase capable of catalyzing both the Claisen condensation to form new C–C bonds and the α-hydroxylation of the amino acid residue in the resonance-stabilized quininoids II and III (Fig. 3). As the active form of vitamin B6, pyridoxal 5-phosphate is a cofactor for a great variety of enzymes catalyzing a long list of reaction processes, including primarily the transamination or desamination, decarboxylation, and racemization of α-amino acids (42). However, CuaB is functionally distinct from the elsewhere-sourced homologs such as the plant prokaryotic-type enzyme with aspartate and prephenate aminotransferase activities (43) and L-aspartate 4-decarboxylase catalyzing the aspartate decarboxylation and transamination reactions (44). This agrees with the phylogenetic analysis of CuaB and its homologs, establishing its distinctness as a bifunctional aminotransferase (Fig. 6).

As an efficient way of obtaining new bioactive natural products, the genome mining effort can be facilitated by the BGC organization of almost all types of compounds such as meroterpenoids (45). This strategy enables as well the characterization of structurally diverse secondary metabolites encoded by orphan and neglected biosynthetic gene clusters (46). Herein, we used the genome mining approach to identify a cryptic *bip* gene cluster in *B. maydis* ATCC48331 under the inspiration of the particular function of CuaB as a PLP-dependent aminotransferase. Activation of the silent *bip* cluster resulted in a family of previously uncharacterized polyketide alkaloids, including bipolamine G (**20**) which is more antibacterial than curvulamine (**1**).

Conclusion

In summary, we have clarified the construction of the indolizidine-coined framework in the curvulamine (**1**) biosynthetic pathway in *Curvularia* sp. IFB-Z10, which is regulated by 6 enzymes, including the highly reducing polyketide synthase (CuaA), the PLP-dependent bifunctional aminotransferase (CuaB), the NADPH-dependent dehydrogenase (CuaC), the FAD-dependent monooxygenase (CuaD), the major facilitator superfamily permease (CuaE), and the Zn(II) Cys_6 transcription factor (CuaF). The bifunctional nature of CuaB lies in its PLP-dependent catalysis for the formation of C–C (via Claisen condensation) and C–O bonds in exposure to dioxygen. Using the CuaB function as a beacon to the biosynthesis of curvulamine relatives, our genome mining effort revealed an array of previously undescribed or otherwise overlooked polyketide alkaloids with 1 (bipolamine G, **20**) more antibacterial than curvulamine, from a single silent gene cluster in *B. maydis* ATCC48331. Collectively, the work presents an undescribed biosynthetic pattern for the indolizidine architecture constructions in fungi and adds evidence for the already fascinating catalytic versatility of PLP-dependent enzymes in nature.

Materials and Methods. General materials and methods are summarized in *SI Appendix*, including *SI Appendix*, Figs. S1–S92 and Tables S1–S18.

CCDC numbers of **14**–**22** have been deposited in the Cambridge Crystallographic Data Centre. Sequence accession numbers of *cuaA*–*cuaF* have been deposited in GenBank of NCBI.

In Vitro Enzymatic Assay. CuaA (100 μM) was combined with CuaB or each CuaB mutant (all at 100 μM) to afford a 100-μL assay mixture, to which NADPH (4 mM), acetyl-CoA (2 mM), malonyl-CoA (2 mM), L-alanine (1 mM), and PLP (1 mM) in a 50 mM Tris·HCl buffer (pH 7.2), followed by standing on a water bath at 30 °C for 10 h were added. The reaction of CuaB with **S13** was performed in the 100-μL assay mixture, including 1 mM PLP, 1 mM L-alanine, 500 μM **S13**, 100 μM ACP, 100 μM NpgA, and 100 μM CuaB in 50 mM Tris·HCl buffer (pH 7.2) at 30 °C for 30 min.

The reaction of CuaB (100 μM) with **S5** (500 μM) was allowed in the presence of 1 mM PLP and 1 mM L-alanine in the 50 mM Tris·HCl buffer (pH 7.2) at 30 °C for 1 h. The enzymatic reaction of CuaD (100 μM) with **3** (100 μM) was performed at 30 °C for different time points in the 50 mM PBS buffer (pH 7.2, 100 μL) containing 10 μM FAD and 1 mM NADH.

Antibacterial Assay. The biological evaluation was performed against the anaerobic bacteria isolated from clinic specimens which were stored prior to test at the Department of Clinical Laboratory, The First Affiliated Hospital of Nanjing Medical University, Nanjing, People's Repubic of China. The magnitude of the activity was expressed in terms of minimal inhibitory concentration (MIC) which was determined by a liquid dilution method (96-well plates). Briefly, the precultured bacterial solution (~10^5 colony/mL) was mingled with serial 2-fold dilutions of the test alkaloids. After vibrating the mixture, the 96-well plates were incubated at 37 °C for 24 h. The lowest concentration of the test compound, at which no visual turbidity is discerned, is defined as MIC.

ACKNOWLEDGMENTS. The work was cofinanced by the Ministry of Science & Technology (2018YFC1706200 and 2018ZX09711001-007-004) and National Natural Science Foundation of China grants (81991524, 81530089, and 81673333). We thank Prof. K. Gomi (Tohoku University) for providing *A. oryzae* NSAR1 and expression vectors pTAex3, pUSA, and pAdeA; Prof. Y. Tang (University of California, Los Angeles) for *S. cerevisiae* BJ5454-npgA and expression vector pYET; and B. G. Turgeon (Cornell University) for *B. maydis* ATCC48331.

1. E. C. Barnes, R. Kumar, R. A. Davis, The use of isolated natural products as scaffolds for the generation of chemically diverse screening libraries for drug discovery. *Nat. Prod. Rep.* **33**, 372–381 (2016).
2. D. J. Newman, G. M. Cragg, Natural products as sources of new drugs from 1981 to 2014. *J. Nat. Prod.* **79**, 629–691 (2016).
3. J. P. Michael, Indolizidine and quinolizidine alkaloids. *Nat. Prod. Rep.* **25**, 139–165 (2008).
4. J. P. Michael, "Simple indolizidine and quinolizidine alkaloids" in *The Alkaloids Chemistry and Biology*, H.-J. Knölker, Ed. (Academic Press, 2016), pp. 1–498.
5. S. Chen *et al*., New regio- and stereoselective cascades via unstabilized azomethine ylide cycloadditions for the synthesis of highly substituted tropane and indolizidine frameworks. *J. Am. Chem. Soc.* **138**, 12664–12670 (2016).
6. D. Mebs, W. Pogoda, S. W. Toennes, Loss of skin alkaloids in poison toads, *Melanophryniscus klappenbachi* (Anura: Bufonidae) when fed alkaloid-free diet. *Toxicon* **150**, 267–269 (2018).
7. T. Grant, P. Colombo, L. Verrastro, R. A. Saporito, The occurrence of defensive alkaloids in non-integumentary tissues of the Brazilian red-belly toad *Melanophryniscus simplex* (Bufonidae). *Chemoecology* **22**, 169–178 (2012).
8. X. Xu, L. Zhang, X. Liu, L. Pan, Q. Liu, Facile [7C+1C] annulation as an efficient route to tricyclic indolizidine alkaloids. *Angew. Chem. Int. Ed. Engl.* **52**, 9271–9274 (2013).
9. D. Kalaitzakis, M. Triantafyllakis, M. Sofiadis, D. Noutsias, G. Vassilikogiannakis, Photooxygenation of furylalkylamines: Easy access to pyrrolizidine and indolizidine scaffolds. *Angew. Chem. Int. Ed. Engl.* **55**, 4605–4609 (2016).
10. H. E. Ho, M. J. James, P. O'Brien, R. J. K. Taylor, W. P. Unsworth, Ag(I)-catalyzed synthesis of azabicyclic alkaloid frameworks from ketimine-tethered ynones: Total synthesis of indolizidine 209D. *Org. Lett.* **20**, 1439–1443 (2018).
11. S. Bunsupa, M. Yamazaki, K. Saito, Lysine-derived alkaloids: Overview and update on biosynthesis and medicinal applications with emphasis on quinolizidine alkaloids. *Mini Rev. Med. Chem.* **17**, 1002–1012 (2017).
12. M. Hartmann, J. Zeier, l-lysine metabolism to N-hydroxypipecolic acid: An integral immune-activating pathway in plants. *Plant J.* **96**, 5–21 (2018).
13. W. Huang, S. J. Kim, J. Liu, W. Zhang, Identification of the polyketide biosynthetic machinery for the indolizidine alkaloid cyclizidine. *Org. Lett.* **17**, 5344–5347 (2015).
14. H. Peng *et al*., Deciphering piperidine formation in polyketide-derived indolizidines reveals a thioester reduction, transamination, and unusual imine reduction process. *ACS Chem. Biol.* **11**, 3278–3283 (2016).
15. U. R. Awodi, J. L. Ronan, J. Masschelein, E. L. C. de Los Santos, G. L. Challis, Thioester reduction and aldehyde transamination are universal steps in actinobacterial polyketide alkaloid biosynthesis. *Chem. Sci.* **8**, 411–415 (2017).
16. D. Cook *et al*., Swainsonine biosynthesis genes in diverse symbiotic and pathogenic fungi. *G3 (Bethesda)* **7**, 1791–1797 (2017).
17. W. B. Han *et al*., Curvulamine, a new antibacterial alkaloid incorporating two undescribed units from a *Curvularia species*. *Org. Lett.* **16**, 5366–5369 (2014).
18. W. B. Han, A. H. Zhang, X. Z. Deng, X. Lei, R. X. Tan, Curindolizine, an anti-inflammatory agent assembled via michael addition of pyrrole alkaloids inside fungal cells. *Org. Lett.* **18**, 1816–1819 (2016).
19. K. Blin *et al*., antiSMASH 5.0: Updates to the secondary metabolite genome mining pipeline. *Nucleic Acids Res.* **47**, W81–W87 (2019).
20. Q. Li *et al*., Deciphering the biosynthetic origin of L-*allo*-isoleucine. *J. Am. Chem. Soc.* **138**, 408–415 (2016).
21. F. J. Jin, J. Maruyama, P. R. Juvvadi, M. Arioka, K. Kitamoto, Development of a novel quadruple auxotrophic host transformation system by *argB* gene disruption using *adeA* gene and exploiting adenine auxotrophy in *Aspergillus oryzae*. *FEMS Microbiol. Lett.* **239**, 79–85 (2004).
22. Y. Matsuda, T. Wakimoto, T. Mori, T. Awakawa, I. Abe, Complete biosynthetic pathway of anditomin: Nature's sophisticated synthetic route to a complex fungal meroterpenoid. *J. Am. Chem. Soc.* **136**, 15326–15336 (2014).
23. S. M. Ma *et al*., Complete reconstitution of a highly reducing iterative polyketide synthase. *Science* **326**, 589–592 (2009).
24. A. T. Keatinge-Clay, The structures of type I polyketide synthases. *Nat. Prod. Rep.* **29**, 1050–1073 (2012).
25. L. Du, L. Lou, PKS and NRPS release mechanisms. *Nat. Prod. Rep.* **27**, 255–278 (2010).
26. M. De Rosa, D. Arnold, Aromaticity and aminopyrroles: Desmotropy and solution tautomerism of 1*H*-pyrrol-3-aminium and 1*H*-pyrrol-3(2*H*)-iminium cation: A stable σ-complex. *J. Org. Chem.* **78**, 1107–1112 (2013).
27. D. J. Miller, Y. M. Zhang, C. O. Rock, S. W. White, Structure of RhlG, an essential beta-ketoacyl reductase in the rhamnolipid biosynthetic pathway of Pseudomonas aeruginosa. *J. Biol. Chem.* **281**, 18025–18032 (2006).
28. S. P. Webster *et al*., Mechanism of 8-amino-7-oxononanoate synthase: Spectroscopic, kinetic, and crystallographic studies. *Biochemistry* **39**, 516–528 (2000).
29. S. Mo *et al*., Elucidation of the *Streptomyces coelicolor* pathway to 2-undecylpyrrole, a key intermediate in undecylprodiginine and streptorubin B biosynthesis. *Chem. Biol.* **15**, 137–148 (2008).
30. R. Gerber, L. Lou, L. Du, A PLP-dependent polyketide chain releasing mechanism in the biosynthesis of mycotoxin fumonisins in *Fusarium verticillioides*. *J. Am. Chem. Soc.* **131**, 3148–3149 (2009).
31. S. W. Chun, M. E. Hinze, M. A. Skiba, A. R. H. Narayan, Chemistry of a unique polyketide-like synthase. *J. Am. Chem. Soc.* **140**, 2430–2433 (2018).
32. Y. L. Du, K. S. Ryan, Pyridoxal phosphate-dependent reactions in the biosynthesis of natural products. *Nat. Prod. Rep.* **36**, 430–457 (2019).
33. M. Wang, Q. Zhao, Q. Zhang, W. Liu, Differences in PLP-dependent cysteinyl processing lead to diverse S-functionalization of lincosamide antibiotics. *J. Am. Chem. Soc.* **138**, 6348–6351 (2016).
34. Y. Huang *et al*., Pyridoxal-5′-phosphate as an oxygenase cofactor: Discovery of a carboxamide-forming, α-amino acid monooxygenase-decarboxylase. *Proc. Natl. Acad. Sci. U.S.A.* **115**, 974–979 (2018).
35. Y. L. Du *et al*., A pyridoxal phosphate-dependent enzyme that oxidizes an unactivated carbon-carbon bond. *Nat. Chem. Biol.* **12**, 194–199 (2016).
36. L. Han *et al*., *Streptomyces wadayamensis* MppP is a PLP-dependent oxidase, not an oxygenase. *Biochemistry* **57**, 3252–3264 (2018).
37. S. Mann, O. Ploux, Pyridoxal-5′-phosphate-dependent enzymes involved in biotin biosynthesis: Structure, reaction mechanism and inhibition. *Biochim. Biophys. Acta* **1814**, 1459–1466 (2011).
38. H. Ikushiro *et al*., Structural insights into the enzymatic mechanism of serine palmitoyltransferase from *Sphingobacterium multivorum*. *J. Biochem.* **146**, 549–562 (2009).
39. S. Fan *et al*., Structure and function of *Mycobacterium smegmatis* 7-keto-8-aminopelargonic acid (KAPA) synthase. *Int. J. Biochem. Cell Biol.* **58**, 71–80 (2015).
40. Y. Hitomi, T. Takeyasu, M. Kodera, Iron complex-based fluorescent probes for intracellular hydrogen peroxide detection. *Chem. Commun. (Camb.)* **49**, 9929–9931 (2013).
41. N. P. Keller, Fungal secondary metabolism: Regulation, function and drug discovery. *Nat. Rev. Microbiol.* **17**, 167–180 (2019).
42. R. Percudani, A. Peracchi, The B6 database: A tool for the description and classification of vitamin B6-dependent enzymatic activities and of the corresponding protein families. *BMC Bioinf.* **10**, 273 (2009).
43. F. de la Torre, J. El-Azaz, C. Avila, F. M. Cánovas, Deciphering the role of aspartate and prephenate aminotransferase activities in plastid nitrogen metabolism. *Plant Physiol.* **164**, 92–104 (2014).
44. N. C. Wang, C. Y. Lee, Enhanced transaminase activity of a bifunctional L-aspartate 4-decarboxylase. *Biochem. Biophys. Res. Commun.* **356**, 368–373 (2007).
45. X. Zhang *et al*., Genome mining and comparative biosynthesis of meroterpenoids from two phylogenetically distinct fungi. *Angew. Chem. Int. Ed. Engl.* **57**, 8184–8188 (2018).
46. J. Shi *et al*., Comparative genome mining and heterologous expression of an orphan NRPS gene cluster direct the production of ashimides. *Chem. Sci.* **10**, 3042–3048 (2019).